Atmospheric Environment 213 (2019) 55–63

Contents lists available at ScienceDirect

Atmospheric Environment

journal homepage: www.elsevier.com/locate/atmosenv

Vertical characteristics of peroxyacetyl nitrate (PAN) from a 250-m tower in northern China during September 2018

Yulu Qiu[a,b], Weili Lin[c], Ke Li[d], Lei Chen[e], Qing Yao[f], Yingxiao Tang[f], Zhiqiang Ma[a,b,*]

[a] Institute of Urban Meteorology, China Meteorological Administration, Beijing, 100089, China
[b] Beijing Shangdianzi Regional Atmosphere Watch Station, Beijing, China
[c] College of Life & Environmental Science, Minzu University of China, Beijing, 100081, China
[d] John A. Paulson School of Engineering and Applied Sciences, Harvard University, Cambridge, MA, 02138, USA
[e] School of Environmental Science and Engineering, Nanjing University of Information Science & Technology, Nanjing, 210044, China
[f] Tianjin Environmental Meteorology Center, Tianjin, 300074, China

GRAPHICAL ABSTRACT

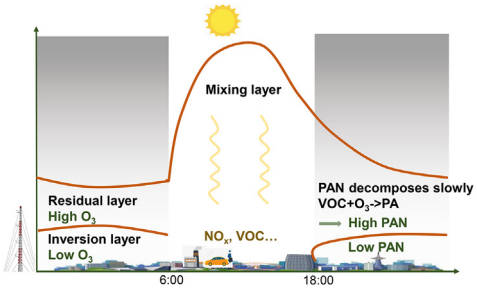

ARTICLE INFO

Keywords:
PAN
Ozone
Vertical characteristics
Northern China

ABSTRACT

Peroxyacetyl nitrate (PAN), formed through photochemical reactions between volatile organic compounds (VOCs) and NO_x, is the second-most important photochemical pollutant. Although several studies have investigated ground-level PAN in northern China, the vertical characteristics of PAN in this region have yet to be examined. In this study, measured concentrations of PAN and ozone (O_3) near the surface and at 220 m were obtained from a 250-m observation tower in Tianjin during September 2018. Results show that the mean PAN concentrations at 220 m are 5.3–19.1% higher than ground-level values during the night (20:00–7:00), which can be attributed to difference in vertical mixing and chemical processes. When the inversion layer is below 220 m, the two layers (220 m and ground level) are separated into the residual layer and inversion layer, between which turbulent exchange is weak. Thus, a vertical gradient for PAN exists during the night. After sunrise, the inversion layer breaks up, and PAN concentrations become more homogeneous due to strong daytime vertical mixing. Role of chemical processes is examined using WRF-Chem model, and it is found that the PAN family—PAN and $CH_3C(O)O_2$ radicals—decompose quickly near the surface in the evening due to strong NO emission sources, while those at 220 m decompose more slowly and could also be produced by the nighttime oxidation between VOCs and O_3. Modeling results further show that nighttime high PAN concentrations in the residual layer can occur throughout all of northern China.

* Corresponding author. Institute of Urban Meteorology, China Meteorological Administration, Beijing, 100089, China.
E-mail address: zqma@ium.cn (Z. Ma).

https://doi.org/10.1016/j.atmosenv.2019.05.066
Received 21 January 2019; Received in revised form 24 May 2019; Accepted 27 May 2019
Available online 28 May 2019
1352-2310/

1. Introduction

In recent years, photochemical pollution in megacities of China has attracted increasing concerns (Xue et al., 2014a, 2014b; Zhang et al., 2014b; Chan et al., 2017; Wang et al., 2017; Li et al., 2019; Qiu et al., 2019). The two most important photochemical pollutants, ozone (O_3) and peroxyacetyl nitrate (PAN), are both formed through photochemical reactions between volatile organic compounds (VOCs) and NO_x ($NO_x \equiv NO + NO_2$). High concentrations of PAN, which have been observed recently in China, have been proved to be responsible for plant injury (Taylor, 1969; Temple and Taylor, 1983) and eye irritation (Heuss and Glasson, 1968). Moreover, PAN becomes rather unstable at high temperatures due to its thermal decomposition property (Seinfeld and Pandis, 2006). Thus, PAN could serve as a reservoir for NO_x in the middle and upper troposphere or at low temperatures (Singh and Hanst, 1981; Singh et al., 1986; Fischer et al., 2010).

Several observational studies conducted in China have examined ground-level PAN features (Liu et al., 2010; Wang et al., 2010; Zhang et al., 2011; Gao et al., 2014; Zhang et al., 2014a; Zhang et al., 2015a; Xu et al., 2015; Zhang et al., 2017). Zhang et al. (2017) analyzed the diurnal variation of PAN concentrations during summer in Beijing from 2006 to 2014 and discovered that PAN concentrations peaked at 14:00 due to the presence of photochemical reactions. By comparing measured PAN concentrations at the suburban site of Lanzhou with values at the remote site of Waliguan in summer 2006, Zhang et al. (2009a) found that the average values of PAN were 0.76 ± 0.89 ppb and 0.44 ± 0.16 ppb, respectively, and concluded that PAN pollution events at Waliguan very likely resulted from the transport of air masses from Lanzhou. By analyzing near-surface PAN in Beijing in August 2007, Liu et al. (2010) demonstrated that the mixing ratios of PAN and O_3 during the day are quite positively correlated. Zhang et al. (2014a), however, reported that a negative correlation existed between PAN and O_3 in Beijing during the winter of 2010, which agrees well with the results of Qiu et al. (2019).

Previous knowledge about PAN in China has been exclusively confined to ground level. Until now, there has been no study exploring the vertical distribution of PAN in China, though a few studies in China have focused on the vertical characteristics of O_3 in the planetary boundary layer (PBL) through the utilization of tower observations (Han et al., 2009; Sun et al., 2010), aircraft (Ding et al., 2008; Chen et al., 2013), and lidar instruments (Ma et al., 2011; Chi et al., 2018). Despite the lack of research concerning the vertical features of PAN in China, there have been several studies investigating the vertical distributions of PAN in other regions (Roberts et al., 2004; Lee et al., 2012). Roberts et al. (2004) investigated the vertical characteristics of PAN in spring of 2002 off the west coast of North America using aircraft observation data and found that PAN showed a slight increase with altitude below 2 km. Using observations and the HYSPLIT model, Lee et al. (2012) concluded that high PAN concentrations were mainly observed in air masses with prior sinking motions within 2 km above sea level. Thus, PAN concentrations below 500 m were clearly lower than those at higher altitudes. This suggests the possibility that PAN concentrations above ground level are very likely to be higher than those near the surface in certain circumstances. As the second most important photochemical pollutant, it is vital to understand PAN's vertical characteristics, especially in polluted urban regions.

Northern China is suffering from serious aerosol pollution (Qiu et al., 2017; Li et al., 2018) and photochemical pollution (Li et al., 2019; Qiu et al., 2019). Tianjin, located about 120 km southeast of Beijing, is one of the megacities in northern China, with a population of more than 15 million at the end of 2016. Like Beijing and Hebei province, Tianjin has been plagued by aerosol pollution in recent years (Han et al., 2012; Zhao et al., 2013; Wang et al., 2014; Zhu et al., 2016; Ding et al., 2018), and it has also been confronted with the challenge of photochemical pollution (Han et al., 2013; Liu et al., 2016; Chen et al., 2018; Li et al., 2019). For example, Li et al. (2019) pointed out that O_3 concentrations at ground level in Beijing-Tianjin-Hebei region exhibited a significant increasing trend of approximately 3 ppb a^{-1} from 2013 to 2017, implying the urgency for future air quality management in this region.

This study, based on measurements from a 250-m tower during September 2018, is the first to present PAN's vertical characteristics in the mixing layer in northern China. The difference and correlation between PAN and O_3 in the vertical direction are presented. We also analyzed the cause of the difference between PAN concentrations near the surface and at 220 m using meteorological parameters and a regional chemical transport model (WRF-Chem). This research aimed to provide information regarding PAN's behavior below the PBL in order to more fully comprehend photochemical levels in Beijing-Tianjin-Hebei region.

2. Methods

2.1. Field observations

In this study, both meteorological and chemical data were used to investigate PAN's vertical characteristics and driving factors. These data were also utilized to evaluate the model performance during the study period. The monitoring station is located in the urban region of Tianjin (39.12°N, 117.17°E, 2.2 m a.s.l.), as shown in Fig. 1. The observation tower top is 250 m. Measurements were taken from September 5–28, 2018.

PAN was measured using an online gas chromatography device equipped with an electron capture detector (GC-3000, FPI Inc., China), with a time resolution of 5 min and a detection limit of 50 ppt. O_3, NO_2, and NO were simultaneously measured with a UV Photometric O_3 Analyzer (Model 49i, Thermo Electron Corporation, USA), a laser-based (cavity-enhanced laser absorption spectroscopy) Nitrogen Dioxide Analyzer (Los Gatos Research, Inc., USA), and a T200U (Teledyne Advanced Pollution Instrumentation) analyzer, respectively. During measurements, air samples at 220 m and 3 m above ground level were alternately measured every 15 min, controlled by a solenoid valve. Air at the 220-m height was drawn down through a teflon pipe (I.D. 32 mm; covered by aluminum foil to avoid sunshine) using a rotary vane vacuum pump with a flow rate of 20 m^3/h. The retention time of the air in the pipe was less than 35 s. The pressure difference between the inlet and outlet of the pipe was less than 20 hPa. We tested ozone concentrations sampled from the inlet and outlet of the pipe from August 16 to September 30, 2017, and the results showed that the O_3 loss was negligible (Fig. 2). Air at the 3-m height was drawn down through a teflon pipe (I.D. 5.3 mm). Routine calibrations of the analyzers were performed during the experiment.

In addition to chemical species, meteorological variables were also observed at 15 platform heights of the tower (5, 10, 20, 30, 40, 60, 80,

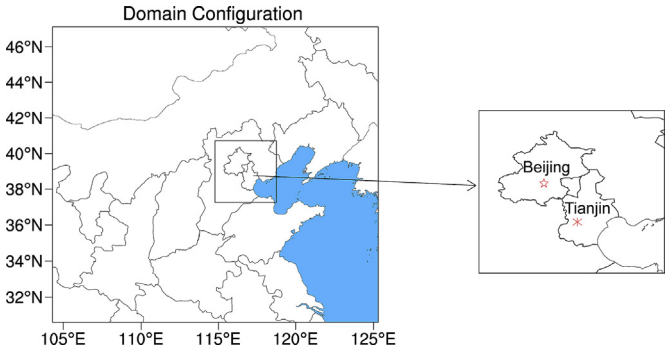

Fig. 1. WRF-Chem model domain configuration (left) and location of the monitoring site in Tianjin (right, red cross). (For interpretation of the references to colour in this figure legend, the reader is referred to the Web version of this article.)

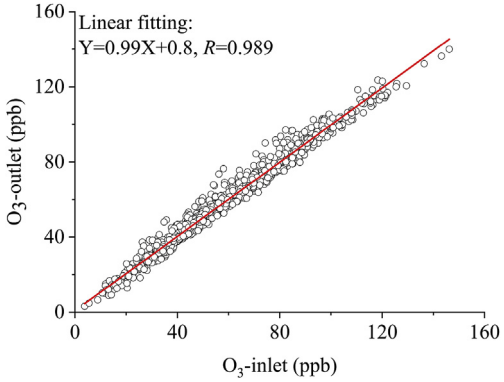

Fig. 2. Relationship between hourly averaged O_3 concentrations sampled from the inlet and outlet of the pipe from August 16 to September 30, 2017.

100, 120, 140, 160, 180, 200, 220, and 250 m). These variables consisted of temperature, relative humidity (RH), wind direction (WD), and wind speed (WS). Hourly averaged data were used in this study. We also calculated the heights of the inversion layer using the observed vertical profiles of temperature, which were determined by the top of the positive temperature vertical gradient level, following the method of Han et al. (2012).

2.2. WRF-Chem model

To determine the cause of the difference between PAN concentrations near the surface and at 220 m, this study utilized the WRF-Chem model, which simultaneously simulates variations of atmospheric chemical species and meteorological fields (Grell et al., 2005; Fast et al., 2006; Chapman et al., 2009). The domain configuration, shown in Fig. 1, covers all of northern China and has a horizontal resolution of 9 km. There are 40 vertical layers in total, including 15 layers below 1 km above the ground, in order to better represent the vertical profiles of atmospheric species in the PBL.

Based on our previous work, the CBM-Z gas-phase scheme (Zaveri and Peters, 1999) performs much better in simulating PAN in northern China than the Regional Acid Deposition Model version 2 (RADM2) gas scheme (Stockwell et al., 1990), due to the discrepancy in calculating reaction rate coefficients of PAN formation through $CH_3C(O)O_2$ (PA) radicals and NO_2 (Qiu et al., 2019). For this reason, we utilized the CBM-Z scheme in this study to simulate PAN. Dry depositions of trace gases and aerosol particles were based on the methods of Wesley (1989) and Binkowski and Shankar (1995), respectively. The detailed chemical and physical schemes adopted in this study are listed in Table 1.

For anthropogenic emissions, we utilized the Multi-resolution Emission Inventory for China (MEIC) for 2012 (http://www.meicmodel.org), which was developed by Tsinghua University (Zhang et al., 2009b; Li et al., 2014; Zheng et al., 2014; Liu et al., 2015). This inventory includes anthropogenic emission rates of SO_2, NO_x, CO, NH_3, VOCs, black carbon (BC), primary organic carbon (POC), primary $PM_{2.5}$, and PM_{10} and has been widely used to simulate aerosols and gas species over northern China (Zhang et al., 2015b; Qiu et al., 2017). Biogenic emissions were calculated online from the Model of Emissions of Gases and Aerosols from Nature (MEGAN) (Guenther et al., 2006).

Table 1
Parameterization schemes used in this study.

	Schemes	References
Chemical schemes		
Gas scheme	CBM-Z	Zaveri and Peters (1999)
Aerosol scheme	MOSAIC-4 bins	Zaveri et al. (2008)
Physical schemes		
Microphysics scheme	WSM 6	Hong and Lim (2006)
Boundary layer scheme	YSU	Hong et al. (2006)
Shortwave radiation scheme	Goddard	Chou et al. (1998)
Longwave radiation scheme	RRTM	Mlawer et al. (1997)
Cumulus scheme	Grell 3D	–

The simulation period extended from September 14, 2018 through September 19, 2018, a time when there was an obvious discrepancy of PAN concentrations between those near the surface and those at 220 m. The first 48 h were considered to be the spin-up time. Therefore, we used simulated results from September 16 to 19 to make the following analysis in this study. The initial and boundary meteorological conditions were provided by the National Centers for Environmental Prediction (NCEP) FNL 1° × 1° reanalysis data. The corresponding conditions for chemical species were from the results of the Whole Atmosphere Community Climate Model (WACCM) (Marsh et al., 2013).

3. Results

3.1. Observed vertical distributions of PAN, O_3, and NO_x

The observation period in this study included almost the entire month of September. In Beijing-Tianjin-Hebei region, September is the transition month when summer ends and fall begins. The Tianjin Meteorological Bureau announced that September 22 was the day on which Tianjin entered into autumn of 2018. Fig. 3 shows the observed time series of temperature, RH, and wind for the two layers in September 2018. Meteorological data in the upper levels of the tower were missing during September 7–16 due to power supply failure. It can be seen that Tianjin was affected by cold air masses around September 6, September 14, and September 21, when temperatures dropped sharply, accompanied by strong northerlies and dry air. After the third temperature drop occurred, Tianjin entered into autumn. Thus, September could indeed be considered as the transition period between summer and autumn.

Fig. 4 shows the observed concentrations of PAN, O_3, NO_2, and NO from the 250-m tower for the period September 5–28, 2018. In general, the O_3 mixing ratios at 220 m were higher than those at ground level, while NO_x concentrations exhibited the opposite behavior. The averaged concentrations for these species during the study period are shown in Table 2. The averaged O_3 concentration at 220 m was 45.6 ppb, which was 31.8% higher than that at ground level. NO_2 had the

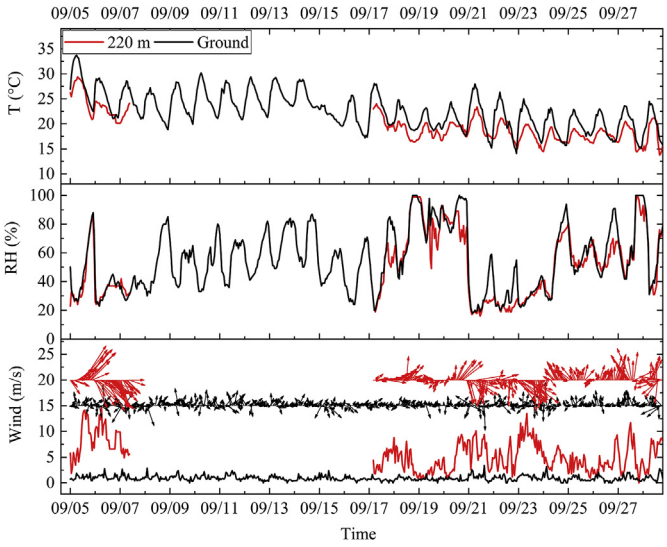

Fig. 3. Observed temperature (°C), RH (%), wind speed (m/s), and wind direction near the surface (black lines) and at 220 m (red lines) from tower observations in Tianjin from September 5–28, 2018. (For interpretation of the references to colour in this figure legend, the reader is referred to the Web version of this article.)

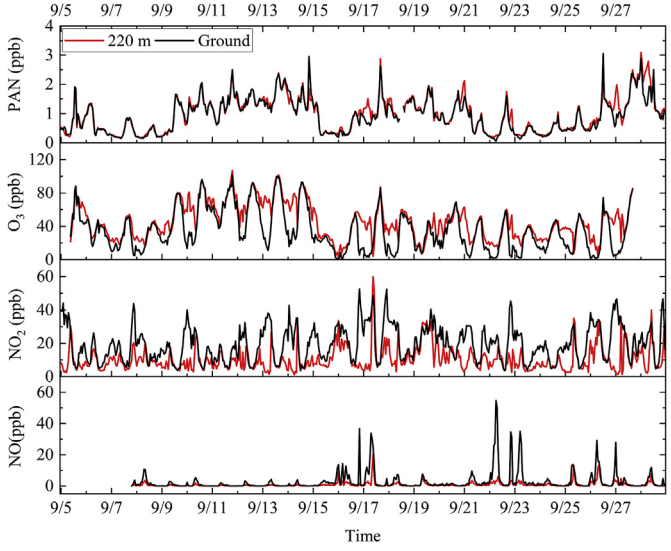

Fig. 4. Observed hourly concentrations (ppb) of PAN, O_3, NO_2, and NO at ground level (black lines) and at 220 m (red lines) in Tianjin from September 5–28, 2018. (For interpretation of the references to colour in this figure legend, the reader is referred to the Web version of this article.)

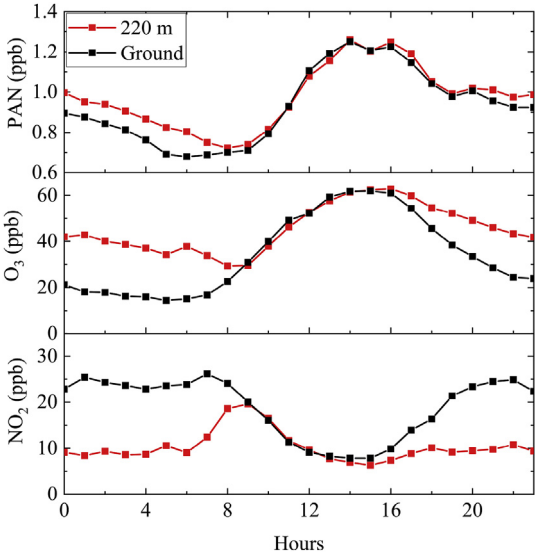

Fig. 5. Observed diurnal cycles of concentrations (ppb) of PAN, O_3, and NO_2 at ground level (black lines) and at 220 m (red lines) averaged from September 5–28, 2018 in Tianjin. (For interpretation of the references to colour in this figure legend, the reader is referred to the Web version of this article.)

Table 2
Statistical results of observed concentrations (ppb) of PAN, O_3, and NO_2 in Tianjin averaged from September 5–28, 2018. The daytime and nighttime periods represent 8:00–19:00 and 20:00–07:00, respectively.

	Period	PAN (ppb)	O_3 (ppb)	NO_2 (ppb)
At ground level	Daytime	1.02 ± 0.58	48.2 ± 22.6	14.3 ± 9.08
	Nighttime	0.84 ± 0.55	20.5 ± 16.3	24.8 ± 9.02
	Average	0.93 ± 0.57	34.6 ± 24.1	19.5 ± 10.4
At 220 m	Daytime	1.03 ± 0.58	50.6 ± 22.1	11.5 ± 8.50
	Nighttime	0.92 ± 0.60	40.6 ± 19.2	9.50 ± 6.03
	Average	0.97 ± 0.59	45.6 ± 21.3	10.5 ± 7.43

opposite spatial relationship, with higher mixing ratios near surface than at higher levels in the PBL, possibly due to the relatively strong NO_x emission source at ground level. For PAN, the difference between its concentration at 220 m and near the surface was smaller than that of other two species, with averaged concentrations at 220 m slightly higher (4.3%) than those at ground level.

Although the mean concentration of PAN at 220 m was only 4.3% higher than that near the surface, the difference between two layers might show obvious diurnal variation. Fig. 5 shows the observed diurnal variations for PAN, O_3 and NO_2 at the two layers averaged over the entire study period. It can be seen that the PAN concentrations at the two levels featured the same general diurnal characteristics, with maximum values at about 14:00. However, PAN concentrations exhibited higher values during the night (20:00–7:00) at 220 m than those at surface. During the day, there was a small discrepancy between PAN concentrations at the two heights due to relatively strong vertical mixing. After reaching a maximum in the afternoon, PAN concentrations near the surface decreased more quickly than those at higher levels. After sunset, the concentration gradient between these two layers increased. The difference of nighttime PAN concentrations between 220 m and near the surface ranged from 0.05 to 0.13 ppb (5.3–19.1%), with mean value of 0.08 ppb (9.5%). The diurnal variation of O_3 was found to be similar to that of PAN. Statistical results showed that nighttime O_3 concentrations at 220 m were 98.0% higher than those at ground level (Table 2). This discrepancy between these two layers was much higher than that of PAN (9.5%). NO_2 exhibited characteristics that were the opposite of the other two species, with higher concentration near the surface due to intensive anthropogenic emissions. The findings associated with NO_2 and O_3 agree well with results previously reported by Han et al. (2009).

3.2. Observed changes of vertical gradients of nighttime PAN, O_3, and NO_2

As mentioned in Section 3.1, the difference of PAN concentrations between two layers was more obvious during the night. Fig. 6 displays the time series of observed vertical gradients for PAN, NO_2, and O_3 concentrations averaged during the night, along with the corresponding inversion layer heights. Results show that the vertical gradients for PAN

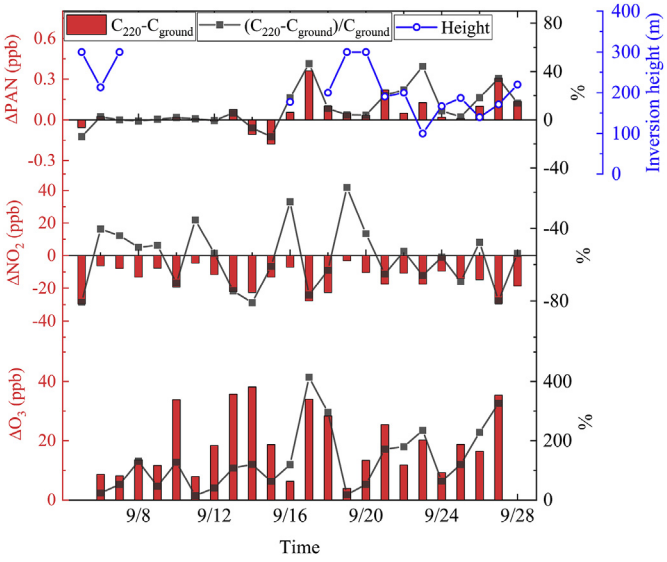

Fig. 6. Time series of vertical gradients between 220 m and ground level for PAN, O_3, and NO_2 averaged during the night (20:00–07:00) in Tianjin from September 5–28, 2018. The red bars and grey lines with solid squares represent absolute (ppb) and relative (%) changes for these species at the two layers, respectively. The blue lines with hollow circles denote the inversion layer height averaged during the night. For inversion heights higher than the tower top (220 m), we considered them to be 300 m in the figure. (For interpretation of the references to colour in this figure legend, the reader is referred to the Web version of this article.)

concentrations between the two layers increased after September 15. In Fig. 6, nighttime vertical gradients for PAN ranged from −0.18 – 0.08 ppb (−13.9–5.7%) before September 15 and increased to 0.01–0.36 ppb (2.4–46.6%) after September 15. Although the absolute vertical gradients of nighttime O_3 concentrations exhibited little change with time, relative values increased noticeably. Nighttime O_3 concentrations at 220 m were 14.9–131.0% higher than those at ground level before September 15, while the ratios increased to 18.0–414.7% after September 15. These ratios were higher than those of PAN. For NO_2, the vertical gradients did not show significant changes with time.

The changes of nighttime vertical gradients of PAN and O_3 concentrations might be related to changes in inversion layer height during the transition season. As shown in Fig. 6, the vertical gradients of PAN and O_3 had generally negative correlations with inversion layer height, although observation data for the inversion layer were missing from September 8–15. This result, in combination with the changes in vertical turbulent exchange associated with the transition from summer to autumn, could account for the vertical gradient variations of O_3. It should be noted that the titration effect for O_3 ($O_3 + NO - - > NO_2 + O_2$) near the surface is much stronger than that at higher levels, which could be attributed to strong sources of NO emissions at ground level (Fig. 4). This phenomenon is more common at night due to the effect of the nocturnal PBL. At night, when the inversion layer is below 220 m, the tower top is in the residual layer. At that time, O_3 at 220 m could maintain its daytime characteristics and thus be less affected by NO emitted from the surface. The difference between O_3 concentrations at 220 m and near the surface could be enhanced by weak vertical mixing. For PAN, vertical gradients were obvious after September 16, especially when the inversion layer heights were lower. In addition to the effect of nocturnal PBL, chemical processes may also play a role. In Sections 3.3 and 3.4, we use the WRF-Chem model to explore this possibility.

3.3. Simulated vertical gradients of nighttime PAN and O_3

The simulated results used here were from September 16–19, when PAN concentrations at 220 m and near the surface exhibited remarkable discrepancies (Fig. 6). Fig. 7 compares simulated and observed concentrations for the two photochemical pollutants from September 16–19. It can be seen that observed nighttime PAN concentrations at 220 m were notably higher than those at ground level on September 16–17 and September 17–18. These were well-captured by the model. The correlation coefficients between simulated and observed PAN at 220 m and near the surface were 0.72 and 0.74, respectively. It should be noted that PAN concentrations at the two levels were both underestimated by approximately 47.5% and 47.2%, respectively. This underestimation in China was also reported by Fischer et al. (2014) and Qiu et al. (2019), and could be the result of uncertainties in VOCs emissions. For O_3, the simulation also showed higher concentrations at higher levels during the night, but failed to capture the peak value on September 17. Statistical results of observed and simulated differences between nighttime PAN concentrations at 220 m and near the surface are listed in Table 3. Overall, the WRF-Chem model could reproduce the positive difference between pollutant concentrations at the two layers during the night, although it underestimated the difference on September 16–17 and overestimated it on September 18–19. During the day, PAN at the two levels showed strong vertical mixing, with differences between the layers being very small in both the observed and simulated results. Although the current model could simulate higher PAN concentration at 220 m during the night, magnitude of the difference between two layers was not accurate enough (Table 3), implying the need of further improvement in the WRF-Chem model. Based on the modeling results, we could perform a diagnostic process analysis using simulated output in order to determine the cause of nighttime vertical gradients.

Table 3
Observed and simulated gradients (ppb) of PAN concentrations between 220 m and ground level during the night in Tianjin. Values in brackets represent relative differences (%).

	Sep 16–17	Sep 17–18	Sep 18–19
Observed PAN	0.36 (46.6%)	0.10 (9.3%)	0.05 (4.0%)
Simulated PAN	0.05 (6.3%)	0.08 (7.8%)	0.18 (13.6%)

3.4. Chemical processes driving nighttime enhancement of vertical gradients of PAN

In the WRF-Chem model, changes in gas concentrations with time could be attributed to changes in chemical reactions, horizontal and vertical advection, vertical mixing, and deposition. The integrated process analysis in the WRF-Chem has been applied in investigating formation of haze and photochemical pollution events in China (Jiang et al., 2012; Gao et al., 2018). Since wet deposition is not included in the simulation due to negligible precipitation during the simulation period, there are only three processes in the simulation, namely, advection, chemical reactions, and vertical mixing (including dry deposition). Given that the WRF-Chem model is capable of simulating the nighttime vertical gradients of PAN, we can utilize the simulation to examine the cause of concentration changes within an hour. Fig. 8

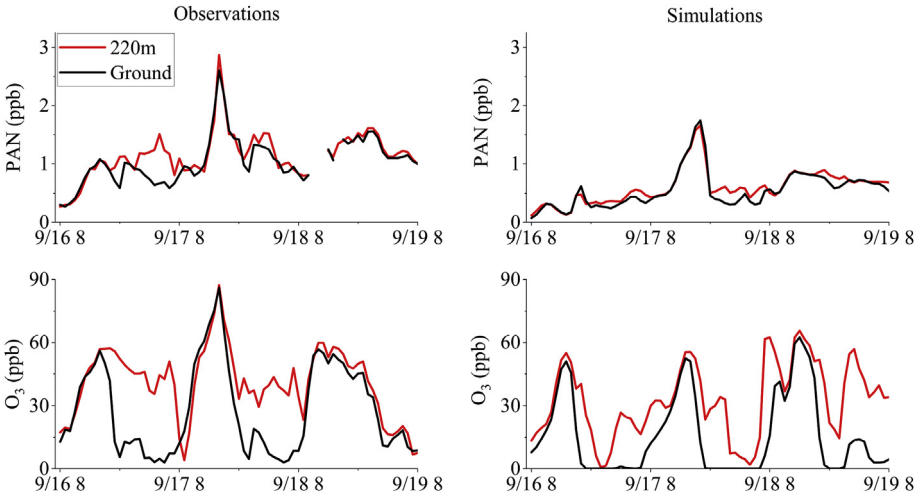

Fig. 7. Observed (left) and simulated (right) time series of PAN and O_3 concentrations (ppb) in Tianjin from September 16–19, 2018.

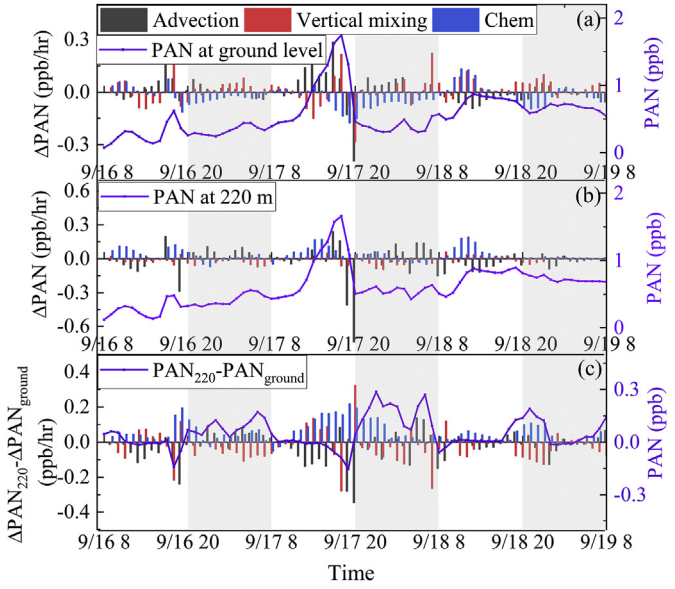

Fig. 8. Simulated changes in PAN concentrations within an hour due to advection (black bars), vertical mixing (red bars), and chemical reactions (blue bars) near the surface (a) and at 220 m (b) in Tianjin from September 16–19, 2018. The purple lines denote the corresponding PAN concentrations. Fig. 8c presents the corresponding difference between Fig. 8b and a. Gray shades denote nighttime periods (20:00–07:00). (For interpretation of the references to colour in this figure legend, the reader is referred to the Web version of this article.)

shows the PAN budget at 220 m and near the surface in Tianjin during the simulation period. It can be seen that the chemical reactions for PAN are, as expected, more intense during the day than at night. The vertical gradient of simulated PAN levels shows an increase in the evening, and is maintained overnight. The diagnostic process analysis in Fig. 8 indicates that the difference between the two layers in the evening and at night may be the result of chemical processes. For example, from nightfall to midnight on September 16, the chemical loss of PAN concentration at ground level ranged from −0.03 – -0.11 ppb/hr, but PAN at 220 m actually exhibited a slight increase over that period. The same phenomenon also occurred on September 17 and September 18 during the simulation period.

3.4.1. Role of different PAN lifetimes

As illustrated above, the difference between PAN concentrations of the two layers during the night could be the result of chemical processes. Chemical processes for PAN and PA radicals consist of formation and decomposition. Thermal decomposition is the main loss pathway for PAN in the PBL (Seinfeld and Pandis, 2006). For PA radicals, it could react readily with NO. The two reactions are as follows:

$$PAN + M \rightarrow PA + NO_2 + M \quad (1)$$

$$PA + NO \rightarrow NO_2 + CH_3O_2 + CO_2 \quad (2)$$

PA radicals can react with NO_2 quickly to form PAN:

$$PA + NO_2 + M \rightarrow PAN + M \quad (3)$$

We considered the lifetime of the PAN family (PA radicals and PAN) in order to better compare the change of PAN levels. Fig. 9 shows the calculated lifetime of the PAN family during the simulation period. The calculation of the PAN family lifetime follows the method in Seinfeld and Pandis (2006):

$$\tau_{PAN} = \frac{1}{k_2[NO]}\left(1 + \frac{k_3[NO_2] + k_2[NO]}{k_1}\right), \quad (4)$$

where k_1, k_2, and k_3 represent the reaction rate coefficients of reactions (1), (2), and (3), respectively. From Eq. (4) we can see that the lifetime of the PAN family is not only determined by rate coefficients but is also affected by the ratios of NO_2/NO and 1/NO. Due to the strong emission source of NO near surface, simulated NO_2/NO ratios at 220 m are several times to thousands of times higher than those at ground level during the night (Fig. 9), leading to the relatively long lifetime of the PAN family at 220 m. This could explain the quicker reduction in PAN concentration near the surface as a result of chemical processes in the evening. For the PAN family at higher levels, existence times could be much longer, and their corresponding concentrations might be higher.

3.4.2. Role of nighttime oxidation of VOCs by O_3

From the diagnostic analysis in Fig. 8, we can also see that weak chemical production at 220 m exists at night. Previous studies (e.g., Fischer et al., 2014), have proven that PA radicals form primarily through the oxidation and photolysis of acetaldehyde (ALD2), acetone (ANO2), and methylglyoxal (MGLY). These reactions, however, generally occur during the day. In addition, PA radicals can be produced from oxidation by NO_3 and O_3 at night (Sander et al., 2006). In this study, we employed the CBM-Z gas-phase scheme, in which reaction rates are determined following the method of Zaveri and Peters (1999).

To confirm the role of NO_3 and O_3 in PA formation during the night at higher levels, we calculated k values and reaction rates of PA formation by NO_3 and O_3 during the night at 220 m using modeling results (Fig. 10). Overall, the calculated k values for OH radicals were largest during the day, with values of approximately 1–3 × 1.0^{-11} cm^3 $molecule^{-1}$ s^{-1}, which were much higher than the nighttime k values of O_3 (0.1–5 × 1.0^{-17} cm^3 $molecule^{-1}$ s^{-1}) and NO_3 (2 × 1.0^{-15} cm^3 $molecule^{-1}$ s^{-1}). However, simulated nighttime NO_3 and O_3 concentrations were much higher than those of the daytime OH radicals. Assuming that all of the VOC species have the same concentration, reaction rates of PA formation for OH are controlled by reaction rates: k[oxidant]. In Fig. 10, calculated k[OH] values are in the range of 4–9 × 1.0^{-13} during the day, while $k[O_3]$ and $k[NO_3]$ are in the range of 0.2–11.0 × 1.0^{-13} and approximately 1.7 × 1.0^{-15} during the night. Thus, oxidation by O_3 might be a possible way to form PAN at 220 m. However, the production of PA due to oxidation by O_3 during the night is still much weaker than the chemical production during the day. The reasons for this are: (1) Only $k[O_3]$ by internal olefin carbons (OLEI) are higher than k[OH]; all of the others have lower values; (2) In addition to oxidation by OH radicals, photolysis of VOC can also produce PA radicals during the day. Since simulated O_3 concentrations are near zero at ground level, the reaction with O_3 of PA formation might be significantly suppressed near the surface. Therefore, the oxidation of VOCs by O_3 during the night could also contribute to some extent to the high PAN levels at 220 m.

4. Discussions and implications

Combining the observation data with the modeling results yields this possible explanation for the difference between PAN concentrations at ground level and the top of the tower (as illustrated in Fig. 11): When the inversion layer builds up in the evening but remains below 220 m during the night, the ground level is in the inversion layer and the tower top is in the residual layer. In this situation, PAN in the inversion layer and in the residual layer would hardly interact with one another. During the evening, the concentrations of PAN and PA radicals at ground level are sharply reduced due to thermal decomposition and reaction with NO, respectively. In the residual layer, however, this decomposition effect becomes less important due to the low NO concentration, and the lifetime of the PAN family is much longer than that near the surface. In addition, there exists weak chemical production of PA radicals due to the reactions of VOCs and O_3 in the residual layer, resulting from high O_3 concentrations in that layer. As such, nighttime PAN concentrations in the residual layer are higher than those at ground level. After sunrise, the inversion layer breaks up, and PAN

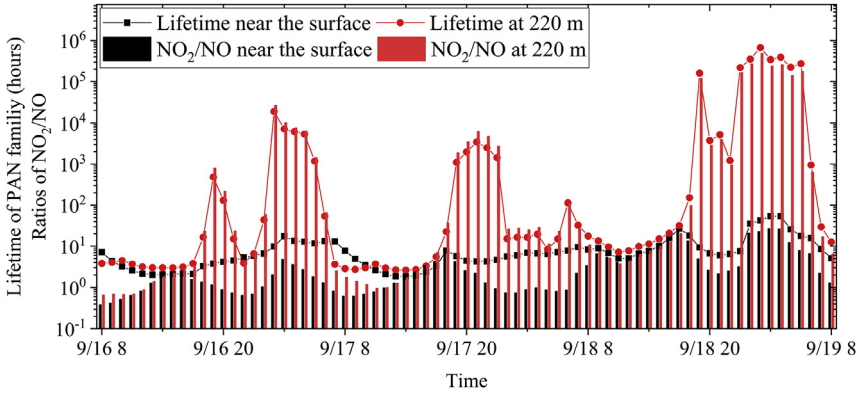

Fig. 9. Calculated lifetime of the PAN family (PA radicals and PAN) (bars) and NO_2/NO ratios (lines) at ground level and at 220 m in the simulation in Tianjin from September 16–19, 2018.

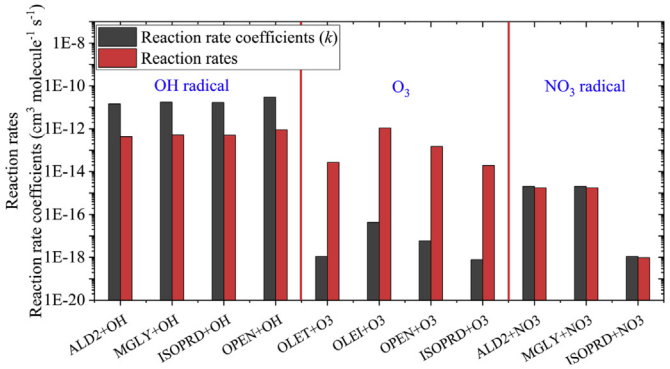

Fig. 10. Comparisons of calculated reaction rate coefficients (k, cm^3 $molecule^{-1}$ s^{-1}) and reaction rates (k[oxidant], ppt cm^3 $molecule^{-1}$ s^{-1}) of PA radical formation through the oxidation by OH (daytime), O_3 (nighttime), and NO_3 (nighttime) at 220 m in the CBM-Z scheme. Here, the concentration of OH radicals at 220 m is the simulated daytime value averaged over September 16–19 in Tianjin, while the NO_3 and O_3 concentrations at 220 m are the simulated nighttime values. The VOCs are assumed to keep constant.

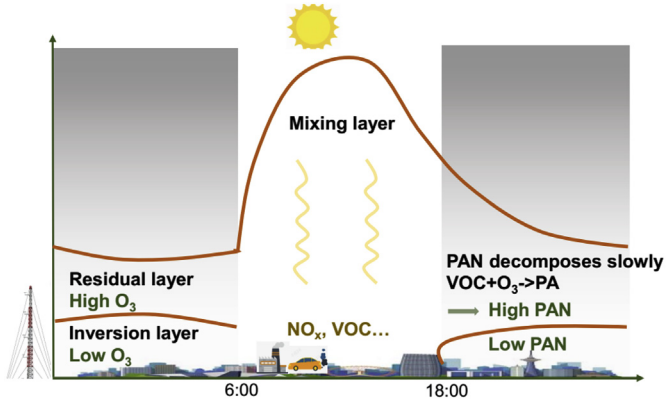

Fig. 11. Schematic diagram of nighttime PAN formation and decomposition in the boundary layer.

concentrations become more homogeneous in the mixing layer.

Since the above results are only for Tianjin, the next question is whether the vertical gradient of PAN occurs across all of northern China. Fig. 12 shows the simulated differences between nighttime PAN concentrations at 220 m and ground level in northern China from September 16–19, 2018. The results indicate that nocturnal PAN concentrations at 220 m exhibited higher levels over most parts of northern China, suggesting that the observed characteristics of the PAN profiles below the PBL might be a common phenomenon across all of northern

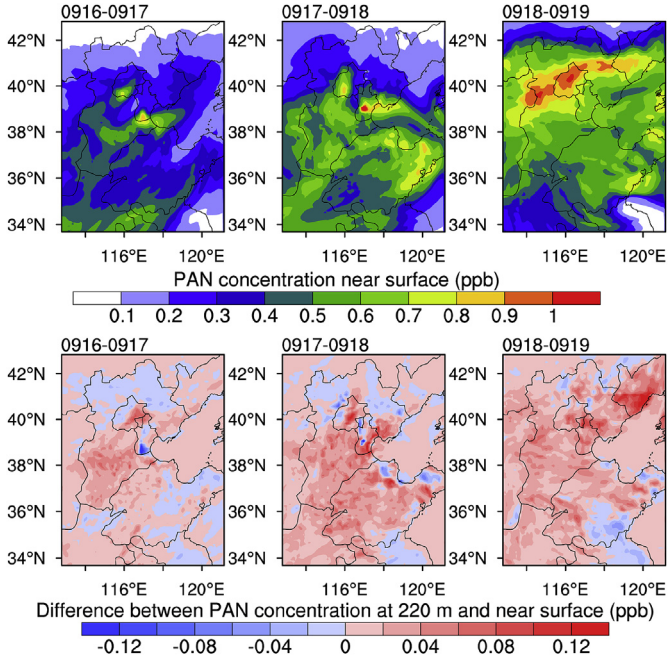

Fig. 12. Simulated daily averaged PAN concentrations near the surface (top, ppb) and differences between PAN concentrations at 220 m and near the surface (bottom, ppb) at night (20:00–07:00) from September 16–19, 2018.

China. In addition, this study also emphasizes the importance of nighttime chemical reactions by O_3 and NO_3 radical in the middle and upper PBL. For O_3, it is not only a photochemical pollutant, but also an oxidant. Although the reaction rate coefficient for O_3 is much smaller compared with other radicals, the relatively higher concentrations might also lead to higher reaction rate.

As shown in Section 3.3, the observed vertical gradient of PAN was underestimated in the model simulation. After investigating the cause of PAN's vertical characteristics below PBL, we find that emission rates of NO_x and simulated O_3 concentrations are both important for simulated differences of PAN concentrations at the two levels. For example, simulated nighttime difference of O_3 concentrations at two layers on Sep 16–17 was 14.7 ppb, which was much lower than observed results (36.7 ppb), thus leading to smaller vertical differences in simulated PAN. Besides, the lifetime of PAN family is very sensitive to NO_x, but the coarse time resolution (monthly) and horizontal resolution ($0.25^\circ \times 0.25^\circ$) of the emission inventory could induce some uncertainties in simulated vertical distributions of PAN with highly spatiotemporal variations. As such, further improvements in emission inventory and representation of other related species (such as O_3 and

NO_x) are needed in better simulating the vertical feature of PAN below PBL.

5. Conclusions

In this study, observed vertical concentrations of PAN, O_3, and NO_x were obtained from a 250-m tower in Tianjin during September 2018. This was the first time that the vertical characteristics of PAN have been reported in China. In addition, we also utilized the WRF-Chem model in order to determine the cause of PAN's vertical characteristics. Our main findings are summarized below.

(1) In general, the observed averaged O_3 mixing ratio at 220 m in September 2018 was 45.6 ppb, which was 31.8% higher than that at ground level. The PAN concentration at 220 m was slightly higher (4.3%) than that at ground level. The differences between the concentrations of PAN and O_3 at 220 m and near the surface were relatively large during the night, with values ranging from 5.3 to 19.1% and 47.0–149.7%, respectively.
(2) The observed vertical gradients of PAN and O_3 concentrations exhibited generally negative correlations with inversion layer height. For PAN, the vertical gradients became large after September 16, especially when the inversion layer height was lower.
(3) Overall, the current WRF-Chem model could reproduce vertical gradients of pollutants at the two layers during nighttime to some extent, though simulated magnitude of the difference should be further improved. Utilizing this model, it was determined that the difference in nighttime PAN concentrations between the two layers might be the result of chemical processes. The shorter lifetime of the PAN family near the surface might explain the quick reduction in PAN concentration due to chemical processes in the evening. In addition, the weak production of PA radicals via reactions between VOCs and O_3 also contributes to some extent to PAN formation at 220 m during the night.
(4) The modeling results indicated that the high PAN concentration in the residual layer is the combined result of weak vertical mixing and chemical production. Further, the modeled high PAN concentration in the residual layer during the night could occur throughout all of northern China. Besides, although the reaction rate coefficient for oxidation by O_3 is much smaller compared with other radicals, the relatively higher concentrations might possibly lead to higher reaction rate in the middle and upper PBL. Further efforts should be made to improve the model performance and investigate the chemical process above the ground.

Conflicts of interest

The authors declared that they have no conflicts of interest to this work.

Acknowledgements

This study was supported by the Beijing Municipal Natural Science Foundation (Grant No. 8194078), the National Natural Science Foundation of China (Grant No. 41475135; 91744206), and the Beijing Nova Program (Grant No. xx2017079). We also acknowledge use of NCAR/ACOM WACCM global model output available at https://www2.acom.ucar.edu/gcm/waccm. All of the observational data and modeling results have been archived by the corresponding author, Prof. Zhiqiang Ma (zqma@ium.cn) and are available upon request.

Appendix A. Supplementary data

Supplementary data to this article can be found online at https://doi.org/10.1016/j.atmosenv.2019.05.066.

References

Binkowski, F.S., Shankar, U., 1995. The regional particulate matter model: 1. Model description and preliminary results. J. Geophys. Res. 100, 26191–26209. https://doi.org/10.1029/95JD02093.
Chan, K.L., Wang, S., Liu, C., Zhou, B., Wenig, M.O., Saiz-Lopez, A., 2017. On the summertime air quality and related photochemical processes in the megacity Shanghai, China. Sci. Total Environ. 580, 974–983. https://doi.org/10.1016/j.scitotenv.2016.12.052.
Chapman, E.G., Gustafson, W.I., Easter, R.C., Barnard, J.C., Ghan, S.J., Pekour, M.S., Fast, J.D., 2009. Coupling aerosol-cloud-radiative processes in the WRF-Chem model: investigating the radiative impact of elevated point sources. Atmos. Chem. Phys. 9, 945–964. https://doi.org/10.5194/acp-9-945-2009.
Chen, L., Guo, B., Huang, J., He, J., Wang, H., Zhang, S., Chen, S., 2018. Assessing air-quality in Beijing-Tianjin-Hebei region: the method and mixed tales of PM2.5 and O3. Atmos. Environ. 193, 290–301. https://doi.org/10.1016/j.atmosenv.2018.08.047.
Chen, P., Quan, J., Zhang, Q., Tie, X., Gao, Y., Li, X., Huang, M., 2013. Measurements of vertical and horizontal distributions of ozone over Beijing from 2007 to 2010. Atmos. Environ. 74 (2), 37–44. https://doi.org/10.1016/j.atmosenv.2013.03.026.
Chi, X., Liu, C., Xie, Z., Fan, G., Wang, Y., He, P., Fan, S., Hong, Q., Wang, Z., Yu, X., Yue, F., Duan, J., Zhang, P., Liu, J., 2018. Observations of ozone vertical profiles and corresponding precursors in the low troposphere in Beijing, China. Atmos. Res. 213, 224–235. https://doi.org/10.1016/j.atmosres.2018.06.012.
Chou, M.D., Suarez, M.J., Ho, C.H., Yan, M.M.H., Lee, K.T., 1998. Parameterizations for cloud overlapping and shortwave single-scattering properties for use in general circulation and cloud ensemble models. J. Clim. 11, 202–214. https://doi.org/10.1175/1520-0442(1998)011<0202:PFCOAS>2.0.CO;2.
Ding, A.J., Wang, T., Thouret, V., Cammas, J.P., Nédélec, P., 2008. Tropospheric ozone climatology over beijing: analysis of aircraft data from the mozaic program. Atmos. Chem. Phys. 8 (1), 1–13. https://doi.org/10.5194/acp-8-1-2008.
Ding, J., Zhang, Y., Han, S., Xiao, Z., Wang, J., Feng, Y., 2018. Chemical, optical and radiative characteristics of aerosols during haze episodes of winter in the North China Plain. Atmos. Environ. 181, 164–176. https://doi.org/10.1016/j.atmosenv.2018.03.006.
Fast, J.D., Gustafson, W.I., Easter, R.C., Zaveri, R.A., Barnard, J.C., Chapman, E.G., Grell, G.A., Peckham, S.E., 2006. Evolution of ozone, particulates, and aerosol direct radiative forcing in the vicinity of Houston using a fully coupled meteorology-chemistry-aerosol model. J. Geophys. Res. 111, D21305. https://doi.org/10.1029/2005JD006721.
Fischer, E.V., Jaffe, D.A., Reidmiller, D.R., Jaeglé, L., 2010. Meteorological controls on observed peroxyacetyl nitrate at Mount Bachelor during the spring of 2008. J. Geophys. Res. 115, D03302. https://doi.org/10.1029/2009JD012776.
Fischer, E.V., Jacob, D.J., Yantosca, R.M., Sulprizio, M.P., Millet, D.B., 2014. Atmospheric peroxyacetyl nitrate (PAN): a global budget and source attribution. Atmos. Chem. Phys. 14, 2679–2698. https://doi.org/10.5194/acp-14-2679-2014.
Gao, J., Zhu, B., Xiao, H., Kang, H., Pan, C., Wang, D., Wang, H., 2018. Effects of black carbon and boundary layer interaction on surface ozone in Nanjing, China. Atmos. Chem. Phys. 18, 7081–7094. https://doi.org/10.5194/acp-18-7081-2018. 2018.
Gao, T., Han, L., Wang, B., Yang, G., Xu, Z., Zeng, L., Zhang, J., 2014. Peroxyacetyl nitrate observed in beijing in August from 2005 to 2009. J. Environ. Sci. 26 (10), 2007–2017. https://doi.org/10.1016/j.jes.2014.08.002.
Grell, G.A., Peckham, S.E., Schmitz, R., McKeen, S.A., Frost, G., Skamarock, W.C., Eder, B., 2005. Fully coupled "online" chemistry within the WRF model. Atmos. Environ. 39, 6957–6975. https://doi.org/10.1016/j.atmosenv.2005.04.027.
Guenther, A., Karl, T., Harley, P., Wiedinmyer, C., Palmer, P.I., Geron, C., 2006. Estimates of global terrestrial isoprene emissions using MEGAN (model of emissions of gases and aerosols from nature). Atmos. Chem. Phys. 6, 3181–3210.
Han, S., Hai, B., Tie, X., Xie, Y., Sun, M., Liu, A., 2009. Impact of nocturnal planetary boundary layer on urban air pollutants: measurements from a 250-m tower over Tianjin, China. J. Hazard Mater. 162, 264–269. https://doi.org/10.1016/j.jhazmat.2008.05.056.
Han, S., Bian, H., Zhang, Y., Wu, J., Wang, Y., Tie, X., Li, Y., Li, X., Yao, Q., 2012. Effect of aerosols on visibility and radiation in spring 2009 in Tianjin, China. Aerosol Air Qual. Res. 12, 211–217. https://doi.org/10.4209/aaqr.2011.05.0073.
Han, S.Q., Zhang, M., Zhao, C.S., Lu, X.Q., Ran, L., Han, M., Li, P.Y., Li, X.J., 2013. Differences in ozone photochemical characteristics between the megacity Tianjin and its rural surroundings. Atmos. Environ. 79, 209–216. https://doi.org/10.1016/j.atmosenv.2013.06.045.
Heuss, J.M., Glasson, W.A., 1968. Hydrocarbon reactivity and eye irritation. Environ. Sci. Technol. 2 (12), 1109–1116.
Hong, S.Y., Lim, J.J., 2006. The WRF single-Moment 6-class microphysics Scheme. J. Korean Meteorl. Soc. 42, 129–151.
Hong, S.Y., Noh, Y., Dudhia, J., 2006. A new vertical diffusion package with an explicit treatment of entrainment processes. Mon. Weather Rev. 134, 2318–2341. https://doi.org/10.1175/MWR3199.1.
Jiang, F., Zhou, P., Liu, Q., Wang, T., Zhuang, B., Wang, X., 2012. Modeling tropospheric ozone formation over East China in springtime. J. Atmos. Chem. 69, 303–319. https://doi.org/10.1007/s10874-012-9244-3. 2012.
Lee, G., Choi, H.S., Lee, T., Choi, J., Park, J.S., Ahn, J.Y., 2012. Variations of regional background peroxyacetyl nitrate in marine boundary layer over Baengyeong Island, South Korea. Atmos. Environ. 61, 533–541. https://doi.org/10.1016/j.atmosenv.2012.07.075.
Li, K., Liao, H., Cai, W., Yang, Y., 2018. Attribution of anthropogenic influence on atmospheric patterns conducive to recent most severe haze over eastern China. Geophys. Res. Lett. 45, 2072–2081. https://doi.org/10.1002/2017GL076570.

Li, K., Jacob, D.J., Liao, H., Shen, L., Zhang, Q., Bates, K.H., 2019. Anthropogenic drivers of 2013-2017 trends in summer surface ozone in China. Proc. Natl. Acad. Sci. 116 (2), 422–427. https://doi.org/10.1073/pnas.1812168116.

Li, M., Zhang, Q., Streets, D.G., He, K.B., Cheng, Y.F., Emmons, L.K., Huo, H., Kang, S.C., Lu, Z., Shao, M., Su, H., Yu, X., Zhang, Y., 2014. Mapping Asian anthropogenic emissions of non-methane volatile organic compounds to multiple chemical mechanisms. Atmos. Chem. Phys. 14, 5617–5638. https://doi.org/10.5194/acp-14-5617-2014.

Liu, B., Liang, D., Yang, J., Dai, Q., Bi, X., Feng, Y., Yuan, J., Xiao, Z., Zhang, Y., Xu, H., 2016. Characterization and source apportionment of volatile organic compounds based on 1-year of observational data in Tianjin, China. Environ. Pollut. 218, 757–769. https://doi.org/10.1016/j.envpol.2016.07.072.

Liu, F., Zhang, Q., Tong, D., Zheng, B., Li, M., Huo, H., He, K.B., 2015. High-resolution inventory of technologies, activities, and emissions of coal-fired power plants in China from 1990 to 2010. Atmos. Chem. Phys. 15, 13299–13317. https://doi.org/10.5194/acp-15-13299-2015.

Liu, Z., Wang, Y., Gu, D., Zhao, C., Huey, L.G., Stickel, R., Liao, J., Shao, M., Zhu, T., Zeng, L., Liu, S.C., Chang, C.C., Amoroso, A., Costabile, F., 2010. Evidence of reactive aromatics as a major source of peroxyacetyl nitrate over China. Environ. Sci. Technol. 44 (18), 7017–7022. https://doi.org/10.1021/es1007966.

Ma, Z.Q., Zhang, X.L., Xu, J., Zhao, X.J., Meng, W., 2011. Characteristics of ozone vertical profile observed in the boundary layer around Beijing in autumn. J. Environ. Sci. 23 (8), 1316–1324. https://doi.org/10.1016/S1001-0742(10)60557-8.

Marsh, D.R., Mills, M.J., Kinnison, D.E., Lamarque, J.F., Calvo, N., Polvani, L.M., 2013. Climate change from 1850 to 2005 simulated in CESM1(WACCM). J. Clim. 26 (19), 7372–7391. https://doi.org/10.1175/jcli-d-12-00558.1.

Mlawer, E.J., Taubman, S.J., Brown, P.D., Iacono, M.J., Clough, S.A., 1997. Radiative transfer for inhomogeneous atmospheres: RRTM, a validated correlated-k model for the longwave. J. Geophys. Res. Atmos. 102, 16663–16682. https://doi.org/10.1029/97JD00237.

Qiu, Y., Liao, H., Zhang, R., Hu, J., 2017. Simulated impacts of direct radiative effects of scattering and absorbing aerosols on surface-layer aerosol concentrations in China during a heavily polluted event in February 2014. J. Geophys. Res. 122, 5955–5975. https://doi.org/10.1002/2016JD026309.

Qiu, Y., Ma, Z., Li, K., 2019. A modeling study of the peroxyacetyl nitrate (PAN) during a wintertime haze event in Beijing, China. Sci. Total Environ. 650, 1944–1953. https://doi.org/10.1016/j.scitotenv.2018.09.253.

Roberts, J.M., Flocke, F., Chen, G., Gouw, J., Holloway, J.S., Hübler, G., Neuman, J.A., Nicks, D.K., Nowak, J.B., Parrish, D.D., Ryerson, T.B., Sueper, D.T., Warneke, C., Fehsenfeld, F.C., 2004. Measurement of peroxycarboxylic nitric anhydrides (PANs) during the ITCT 2K2 aircraft intensive experiment. J. Geophys. Res. 109, D23S21. https://doi.org/10.1029/2004JD004960.

Sander, S.P., Friedl, R.R., Golden, D.M., et al., 2006. Chemical Kinetics and Photochemical Data for Use in Atmospheric Studies Evaluation Number 15. Jet Propulsion Laboratory Publication 06-2.

Seinfeld, J.H., Pandis, S.N., 2006. Atmospheric Chemistry and Physics: from air pollution to climate change. https://doi.org/10.1063/1.882420.

Singh, H.B., Hanst, P.L., 1981. Peroxyacetyl nitrate (PAN) in the unpolluted atmosphere: an important reservoir for nitrogen oxides. Geophys. Res. Lett. 8, 941–944.

Singh, H.B., Salas, L.J., Viezee, W., 1986. Global distribution of peroxyacetyl nitrate. Nature 321 (5), 588–591.

Stockwell, W.R., Middleton, P., Chang, J.S., 1990. The second generation regional acid deposition model: chemical mechanism for regional air quality modeling. J. Geophys. Res. 95, 16343–16367.

Sun, Y., Wang, Y., Zhang, C., 2010. Vertical observations and analysis of PM2.5, O3, and NOx at Beijing and Tianjin from towers during summer and autumn 2006. Adv. Atmos. Sci. 27 (1), 123–136. https://doi.org/10.1007/s00376-009-8154-z.

Taylor, O.C., 1969. Importance of peroxyacetyl nitrate (PAN) as a phytotoxic air pollutant. J. Air Pollut. Control Assoc. 19, 347–351. https://doi.org/10.1080/00022470.1969.10466498.

Temple, P.J., Taylor, O.C., 1983. World-wide ambient measurements of peroxyacetyl nitrate (PAN) and implications for plant injury. Atmos. Environ. 17 (8), 1583–1587.

Wang, B., Shao, M., Roberts, J.M., Yang, G., Yang, F., Hu, M., Zeng, L., Zhang, Y., Zhang, J., 2010. Ground-based on-line measurements of peroxyacetyl nitrate (PAN) and peroxypropionyl nitrate (PPN) in the Pearl River Delta, China. Int. J. Environ. Anal. Chem. 90 (7), 548–559. https://doi.org/10.1080/03067310903194972.

Wang, Y.S., Yao, L., Wang, L.L., Liu, Z.R., Ji, D.S., Tang, G.Q., Zhang, J.K., Sun, Y., Hu, B., Xin, J.Y., 2014. Mechanism for the formation of the January 2013 heavy haze pollution episode over central and eastern China. Sci. China Earth Sci. 57, 14–25. https://doi.org/10.1007/s11430-013-4773-4.

Wang, T., Xue, L., Brimblecombe, P., Lam, Y.F., Li, L., Zhang, L., 2017. Ozone pollution in China: a review of concentrations, meteorological influences, chemical precursors, and effects. Sci. Total Environ. 575 (2017), 1582–1596. https://doi.org/10.1016/j.scitotenv.2016.10.081.

Wesley, M.L., 1989. Parameterization of surface resistance to gaseous dry deposition in regional numerical models. Atmos. Environ. 23, 1293–1304. https://doi.org/10.1016/0004-6981(89)90153-4.

Xu, Z., Xue, L., Wang, T., Xia, T., Gao, Y., Louie, P.K., Luk, C.W., 2015. Measurements of peroxyacetyl nitrate at a background site in the Pearl River delta region: production efficiency and regional transport. Aerosol Air Qual. Res. 15 (1), 833–841.

Xue, L., Wang, T., Gao, J., Ding, A.J., Zhou, X.H., Blake, D.R., Wang, X.F., Saunders, S.M., Fan, S.J., Zuo, H.C., Zhang, Q.Z., Wang, W.X., 2014a. Ground-level ozone in four Chinese cities: precursors, regional transport and heterogeneous processes. Atmos. Chem. Phys. 14 (23), 13175–13188. https://doi.org/10.5194/acp-14-13175-2014.

Xue, L., Wang, T., Wang, X., Blake, D., Gao, J., Nie, W., Gao, R., Gao, X., Xu, Z., Ding, A., Huang, Y., Lee, S., Chen, Y., Wang, S., Chai, F., Zhang, Q., Wang, W., 2014b. On the use of an explicit chemical mechanism to dissect peroxy acetyl nitrate formation. Environ. Pollut. 195 (36), 39–47. https://doi.org/10.1016/j.envpol.2014.08.005.

Zaveri, R.A., Peters, L.K., 1999. A new lumped structure photochemical mechanism for large-scale applications. J. Geophys. Res. 104, 30,387–30,415. https://doi.org/10.1029/1999JD900876.

Zaveri, R.A., Easter, R.C., Fast, J.D., Peters, L.K., 2008. Model for simulating aerosol interactions and chemistry (MOSAIC). J. Geophys. Res. 113, D13204. https://doi.org/10.1029/2007JD008782.

Zhang, J.M., Wang, T., Ding, A.J., Zhou, X.H., Xue, L.K., Poon, C.N., Wu, W.S., Gao, J., Zuo, H.C., Chen, J.M., Zhang, X.C., Fan, S.J., 2009a. Continuous measurement of peroxyacetyl nitrate (PAN) in suburban and remote areas of western China. Atmos. Environ. 43 (2), 228–237. https://doi.org/10.1016/j.atmosenv.2008.09.070.

Zhang, Q., Streets, D.G., Carmichael, G.R., He, K.B., Huo, H., Kannari, A., Klimont, Z., Park, I.S., Reddy, S., Fu, J.S., Chen, D., Duan, L., Lei, Y., Wang, L.T., Yao, Z.L., 2009b. Asian emissions in 2006 for the NASA INTEX-B mission. Atmos. Chem. Phys. 9, 5131–5153.

Zhang, J.B., Xu, Z., Yang, G., Wang, B., 2011. Peroxyacetyl nitrate (PAN) and peroxypropionyl nitrate (PPN) in urban and suburban atmospheres of Beijing, China. Atmos. Chem. Phys. Discuss. 11, 8173–8206. https://doi.org/10.5194/acpd-11-8173-2011.

Zhang, H., Xu, X., Lin, W., Wang, Y., 2014a. Wintertime peroxyacetyl nitrate (PAN) in the megacity Beijing: role of photochemical and meteorological processes. J. Environ. Sci. 26 (1), 83–96.

Zhang, Q., Yuan, B., Shao, M., Wang, X., Lu, S., Lu, K., Wang, M., Chen, L., Chang, C.C., Liu, S.C., 2014b. Variations of ground-level O3 and its precursors in Beijing in summertime between 2005 and 2011. Atmos. Chem. Phys. 14 (12), 6089–6101. https://doi.org/10.5194/acp-14-6089-2014.

Zhang, G., Mu, Y., Zhou, L., Zhang, C., Zhang, Y., Liu, J., Fang, S., Yao, B., 2015a. Summertime distributions of peroxyacetyl nitrate (PAN) and peroxypropionyl nitrate (PPN) in Beijing: understanding the sources and major sink of PAN. Atmos. Environ. 103, 289–296. https://doi.org/10.1016/j.atmosenv.2014.12.035.

Zhang, L., Wang, T., Lv, M., Zhang, Q., 2015b. On the severe haze in Beijing during January 2013: unraveling the effects of meteorological anomalies with. WRF-Chem. Atmos. Environ. 104 (2015), 11–21. https://doi.org/10.1016/j.atmosenv.2015.01.001.

Zhang, B., Zhao, B., Zuo, P., Huang, Z., Zhang, J., 2017. Ambient peroxyacyl nitrate concentration and regional transportation in Beijing. Atmos. Environ. 166, 543–550. https://doi.org/10.1016/j.atmosenv.2017.07.053.

Zhao, X.J., Zhao, P.S., Xu, J., Meng, W., Pu, W.W., Dong, F., He, D., Shi, Q.F., 2013. Analysis of a winter regional haze event and its formation mechanism in the North China Plain. Atmos. Chem. Phys. 13, 5685–5696. https://doi.org/10.5194/acp-13-5685-2013.

Zheng, B., Huo, H., Zhang, Q., Yao, Z.L., Wang, X.T., Yang, X.F., Liu, H., He, K.B., 2014. High-resolution mapping of vehicle emissions in China in 2008. Atmos. Chem. Phys. 14, 9787–9805. https://doi.org/10.5194/acp-14-9787-2014.

Zhu, X., Tang, G., Hu, B., Wang, L., Xin, J., Zhang, J., Liu, Z., Münkel, C., Wang, Y., 2016. Regional pollution and its formation mechanism over North China Plain: a case study with ceilometer observations and model simulations. J. Geophys. Res. Atmos. 121, 14,574–14,588. https://doi.org/10.1002/2016JD025730.